Proton-Coupled Electron Transfer in a Biomimetic Peptide as a Model of Enzyme Regulatory Mechanisms

Robin Sibert,[†,‡] Mira Josowicz,[†] Fernando Porcelli,[§,∥] Gianluigi Veglia,[§]
Kevin Range,[⊥] and Bridgette A. Barry*[†,‡]

Contribution from the Department of Chemistry and Biochemistry and the Petit Institute for Bioengineering and Bioscience, Georgia Institute of Technology, Atlanta, Georgia 30332, Department of Biochemistry, Molecular Biology, and Biophysics and the Department of Chemistry, University of Minnesota, Minneapolis, Minnesota 55415, Department of Environmental Sciences, University of Tuscia, Viterbo, Italy, and Department of Chemistry, Lock Haven University of Pennsylvania, Lock Haven, Pennsylvania 17745

Received December 8, 2006; E-mail: Bridgette.Barry@Chemistry.Gatech.Edu

Abstract: Proton-coupled electron-transfer reactions are central to enzymatic mechanism in many proteins. In several enzymes, essential electron-transfer reactions involve oxidation and reduction of tyrosine side chains. For these redox-active tyrosines, proton transfer couples with electron transfer, because the phenolic pK_A of the tyrosine is altered by changes in the tyrosine redox state. To develop an experimentally tractable peptide system in which the effect of proton and electron coupling can be investigated, we have designed a novel amino acid sequence that contains one tyrosine residue. The tyrosine can be oxidized by ultraviolet photolysis or electrochemical methods and has a potential cross-strand interaction with a histidine residue. NMR spectroscopy shows that the peptide forms a β-hairpin with several interstrand dipolar contacts between the histidine and tyrosine side chains. The effect of the cross-strand interaction was probed by electron paramagnetic resonance and electrochemistry. The data are consistent with an increase in histidine pK_A when the tyrosine is oxidized; the effect of this thermodynamic coupling is to increase tyrosyl radical yield at low pH. The coupling mechanism is attributed to an interstrand π–cation interaction, which stabilizes the tyrosyl radical. A similar interaction between histidine and tyrosine in enzymes provides a regulatory mechanism for enzymatic electron-transfer reactions.

Redox-active tyrosine residues mediate long-distance electron-transfer reactions in several enzymes.[1] For example, in photosystem II (PSII), Tyr 161 of the D1 polypeptide (Y_Z) participates in water oxidation by reducing the primary donor P_{680}^+ and by oxidizing the manganese cluster.[2] Tyr 160 in the D2 polypeptide (Y_D) is also redox-active but is not required for water oxidation {reviewed in ref 3}. In addition to Y_Z in PSII, tyrosyl radicals are essential for catalytic activity of prostaglandin H synthase,[4] ribonucleotide reductase (RNR),[5] and galactose oxidase.[6] Elucidation of the environmental factors, which influence the structure and function of the radical, will provide insights into the control of the activity in these enzymes.

EPR studies of isotopically labeled tyrosinate have revealed that tyrosine oxidation occurs from the aromatic ring, generating a neutral radical with spin density located on the 1′, 3′, and 5′ carbon atoms and on the phenolic oxygen.[7,8] Additionally, rotation around the $C_{1'}$–C_β bond alters the EPR line shape.[7,8] In dipeptides, pentapeptides, and PSII, evidence for spin density delocalization to the amide group has been obtained {see ref 9 and references therein}. Oxidation of a protonated tyrosine at neutral pH values is coupled with the deprotonation of the phenolic oxygen.[10] This coupling of electron and proton transfer is due to a dramatic decrease in the pK_A of the phenolic oxygen in the radical state.[10] Therefore, changes in the pK_A of the proton-accepting group can alter the free energy of the oxidation/reduction reaction.[11] In direct coupling reactions, the proton and electron movement may be simultaneous, sequential, or nonsynchronous.[12]

[†] Department of Chemistry and Biochemistry, Georgia Institute of Technology.
[‡] Petit Institute for Bioengineering and Bioscience, Georgia Institute of Technology.
[§] University of Minnesota.
[∥] University of Tuscia.
[⊥] Lock Haven University of Pennsylvania.

(1) Barry, B. A.; Einarsdottir, O. *J. Phys. Chem. B* **2005**, *109*, 6972−6981.
(2) Britt, R. D. In *Oxygenic Photosynthesis: The Light Reactions*; Ort, D. R., Yocum, C. F., Eds.; Kluwer Academic Publisher: Dordrecht, 1996; Vol. 4, pp 137−164.
(3) Pujols-Ayala, I.; Barry, B. A. *Biochim. Biophys. Acta* **2004**, *1655*, 205−216.
(4) Malkowski, M. G. G., S. L.; Smith, W. L.; Garavito, R. M. *Science* **2000**, *289*, 1933−1937.
(5) Stubbe, J.; van Der Donk, W. A. *Chem. Rev.* **1998**, *98*, 705−762.
(6) Whittaker, M. M.; Whittaker, J. W. *J. Biol. Chem.* **1990**, *265*, 9610−9613.

(7) Barry, B. A.; El-Deeb, M. K.; Sandusky, P. O.; Babcock, G. T. *J. Biol. Chem.* **1990**, *265*, 20139−20143.
(8) Hulsebosch, R. J.; van der Brink, J. S.; Niewenhuis, S. A. M.; Gast, P.; Raap, J.; Lugtenburg, J.; Hoff, A. J. *J. Am. Chem. Soc.* **1997**, *119*, 8685−8694.
(9) Vassiliev, I. R.; Offenbacher, A. R.; Barry, B. A. *J. Phys. Chem. B* **2005**, *109*, 23077−23085.
(10) Dixon, W. T.; Murphy, D. *J. Chem. Soc., Faraday Trans. 2* **1976**, *72*, 1221−1229.
(11) Rhile, I. J.; Markle, T. F.; Nagao, H.; DiPasquale, A. G.; Lam, O. P.; Lockwood, M. A.; Rotter, K.; Mayer, J. M. *J. Am. Chem. Soc.* **2006**, *128*, 6075−6088.

According to Marcus theory, one of the factors influencing the electron-transfer rate is the oxidation potential of the redox-active cofactor.[13] Previous work has reported a shift in tyrosine redox potential in designed helical proteins that contain tyrosine residues.[14,15] In one study, the observed increase was attributed to the nonpolar environment and to shielding of the aromatic side chain from potential proton acceptors.[14] More specific intermolecular interactions with hydrogen bonded and charged groups are also expected to shift the midpoint potential.[11] The effect of noncovalent interactions on the potential of redox-active cofactors, such as hemes, iron sulfur clusters, and other metal centers, has been systematically explored in peptide models or maquettes {for examples, see refs 16–24}. Also, peptide bond formation may change the midpoint potential of a redox active amino acid residue, if spin density delocalization occurs to the peptide bond.[9]

To develop a peptide system in which the effect of specific intermolecular and covalent interactions on tyrosyl radical can be probed, we designed an 18 amino acid sequence (Figure 1A, Peptide A), which we predicted would fold into a β-hairpin polypeptide {for previous examples of designed β-hairpin peptides, see refs 25,26}. This peptide exhibits an interstrand proton-coupled electron-transfer reaction between a histidine and the redox-active tyrosine. Our data suggest that thermodynamic coupling between electron and proton transfer decreases the midpoint potential of the redox-active tyrosine at low pH values.

Materials and Methods

Samples. Peptide A, IMDRYRVRNGDRIHIRLR, and peptide C, IMDRYRVRNGDRIChaIRLR, in which a cyclohexylalanine (Cha) is substituted for a histidine, were synthesized by Sigma Genosys (The Woodlands, Texas). The peptides were purified to 95% homogeneity by the manufacturer. Mass spectrometry was used to verify the sequence, and the purity was determined by analysis of the reversed-phase HPLC chromatogram.

NMR Spectroscopy. The NMR samples had a concentration of 1 mM in 90% ^{1}H$_2$O/10% ^{2}H$_2$O and were buffered with 10 mM sodium phosphate, pH 5.0. NMR spectra were recorded using a Varian Unity spectrometer operating at 600 MHz at a temperature of 25 °C. An inverse detection triple-resonance probe was used. Resonance assignments were performed using two-dimensional ^{1}H/^{1}H TOCSY (75 ms mixing times) and ^{1}H/^{1}H ROESY (100, 200, 350 ms mixing time) experiments.[27] Water suppression was achieved using the WATER-GATE technique.[28] Spectra were collected with 256 complex data points
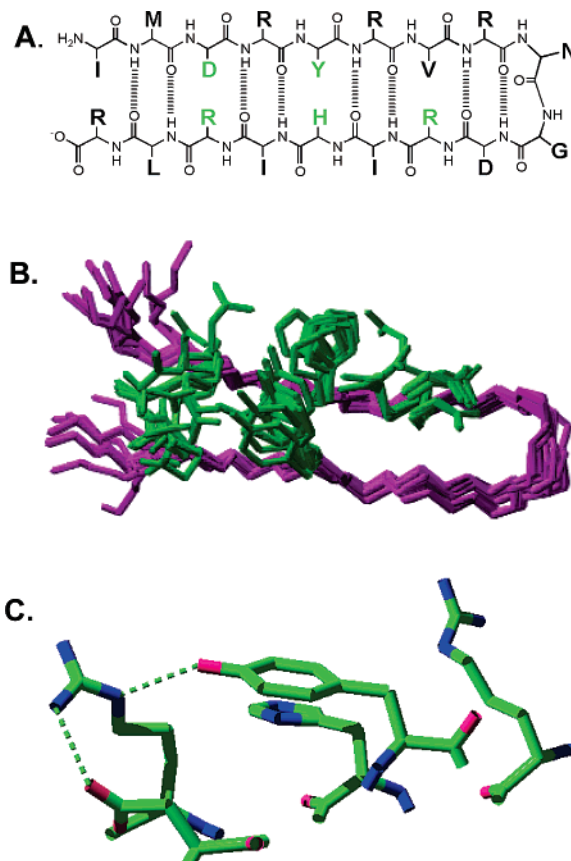

Figure 1. Structures of peptide A, IMDRYRVRNGDRIHIRLR. (A) The primary sequence, predicted hydrogen bonds, and predicted cross-strand interactions with tyrosine (green) are shown. (B) The overlap of the 20 lowest energy structures, as derived from 2-D NMR spectroscopy at pH 5.0, is presented. Only five amino acid side chains (see part A, green) are shown. (C) Interactions with the tyrosine, Y5, in the averaged, minimized NMR structure are shown. Hydrogen atoms are omitted, and hydrogen bonds are shown as dotted lines.

in the t_1 dimension and 1024 in the t_2 dimension. TOCSY spectra were acquired using a DIPSI-2 pulse sequence.[29,30] The spectral widths were 8 kHz on both the t_1 and t_2 dimensions. The DQF-COSY spectrum[31,32] was acquired on the 800 MHz Varian Unity spectrometer using 512 complex data points in the t_1 dimension and 2048 in the t_2 dimension. The DQF-COSY data were apodized with a 90° shifted sine bell in both dimensions prior to zero filling to 2048 × 4096 data matrices to obtain the maximum digital resolution for coupling constant measurements. Proton chemical shifts were referenced to internal 3-(trimethylsilyl)propionic acid (TSPA). NMR spectra were processed using NMRPipe[33] and analyzed using SPARKY.[34] 2D spectra were processed with a sine bell window function shifted by 90°. The data were zero filled to twice their size before Fourier transformation. In the ROESY spectrum obtained with a mixing time of 300 ms, ROE cross-peaks were integrated and used for the structure calculations. The ROE volumes were calibrated using the average ROE volume from resolved aromatic vicinal protons of Tyr5. The ROE volumes were classified as strong, medium, and weak, corresponding to distance restraints of

(12) Chang, C. J.; Chang, M. C. Y.; Damrauer, N. H.; Nocera, D. G. *Biochim. Biophys. Acta* **2004**, *1655*, 13−28.
(13) Marcus, R. A. *Pure Appl. Chem.* **1997**, *69*, 13−29.
(14) Tommos, C. S., J.; Pilloud, D. L.; Wand, A. J.; Dutton, L. P. *Biochemistry* **1999**, *38*, 9495−9507.
(15) Di Bilio, A. J.; Crane, B. R.; Wehbi, W. A.; Kiser, C. N.; Abu-Omar, M. M.; Carlos, R. M.; Richards, J. H.; Winkler, J. R.; Gray, H. B. *J. Am. Chem. Soc.* **2001**, *123*, 3181−3182.
(16) Shifman, J. M.; Moser, C. C.; Kalsbeck, W. A.; Bocian, D. F.; Dutton, P. L. *Biochemistry* **1998**, *37*, 16815−16827.
(17) Jones, G., II; Vullev, V.; Braswell, E. H.; Zhu, D. *J. Am. Chem. Soc.* **2000**, *122*, 388−389.
(18) Lombardi, A.; Nastri, F.; Pavone, V. *Chem. Rev.* **2001**, *101*, 3165−3190.
(19) Gibney, B. R.; Huang, S. S.; Skalicky, J. J.; Fuentes, E. J.; Wand, A. J.; Dutton, P. L. *Biochemistry* **2001**, *40*, 10550−10561.
(20) Kennedy, M. L.; Gibney, B. R. *J. Am. Chem. Soc.* **2002**, *124*, 6826−6827.
(21) Discher, B. M.; Noy, D.; Strzalka, J.; Ye, S.; Moser, C. C.; Lear, J. D.; Blasie, J. K.; Dutton, P. L. *Biochemistry* **2005**, *44*, 12329−12343.
(22) Cochran, F. V.; Wu, S. P.; Wang, W.; Nanda, V.; Saven, J. G.; Therien, M. J.; DeGrado, W. F. *J. Am. Chem. Soc.* **2005**, *127*, 1346−1347.
(23) Shearer, J.; Long, L. M. *Inorg. Chem.* **2006**, *45*, 2358−2360.
(24) Zhuang, J.; Amoroso, J. H.; Kinloch, R.; Dawson, J. H.; Baldwin, M. J.; Gibney, B. R. *Inorg. Chem.* **2006**, *45*, 4685−4694.
(25) Syud, F. A.; Stanger, H. E.; Gelman, S. H. *J. Am. Chem. Soc.* **2001**, *123*, 8667−8677.
(26) Tatko, C.; Waters, M. L. *Protein Sci.* **2003**, *12*, 2443−2452.

(27) Kumar, A.; Ernst, R. R.; Wuthrich, K. *Biochem. Biophys. Res. Commun.* **1980**, *95*, 1−6.
(28) Piotto, M.; Saudek, V.; Sklenar, V. *Biomol. NMR* **1992**, *2*, 661−665.
(29) Bax, A.; David, D. G. *J. Magn. Reson.* **1985**, *65*, 355−360.
(30) Shaka, A. J.; Lee, C. J.; Pines, A. *J. Magn. Reson.* **1998**, *77*, 274−293.
(31) Piantini, U.; Sorensen, O. W.; Ernst, R. R. *J. Am. Chem. Soc.* **1982**, *124*, 6800−6801.
(32) Rance, M.; Sorensen, O. W.; Bodenhausen, G.; Wagner, G.; Ernst, R. R.; Wuthrich, K. *Biochem. Biophys. Res. Commun.* **1983**, *117*, 479−485.
(33) Delaglio, F.; Grzesiek, S.; Vuister, G. W.; Zhu, G.; Pheifer, J.; Bax, A. *J. Biomol. NMR* **1995**, *6*, 277−293.
(34) Goddard, T. D.; Kneller, D. G. *SPARKY 3*; 1999.

1.9−2.7 Å, 1.9−3.3 Å, and 1.9−5.0 Å, respectively.[35] Structure calculations were performed using XPLOR-NIH,[36,37] starting from extended structures and using random simulated annealing calculations.[38] An initial high-temperature phase consisting of 6000 restrained molecular dynamics steps of 0.5 fs each was performed at a temperature of 1000 K. During this stage, all of the force constants were kept fixed. Subsequently, a molecular dynamics cooling phase comprised of 3000 steps of 0.5 fs each was employed, with the temperature decreasing from 1000 to 100 K during this interval. To refine the generated conformers, a second simulated annealing was carried out starting at 2000 K, including the full van der Waals potential. The temperature was decreased from 2000 to 0 K. During the high-temperature steps, the dihedral angles were constrained using a harmonic potential with a force constant of 200 kcal/mol. A final minimization of 500 steps was performed using the Conjugated Gradients Method. A total of 147 ROEs (78 inter- and 69 intraresidue) was used in the calculations. All the ROEs were unambiguously assigned, and since stereospecific assignments could not be made pseudo atoms were employed using the center of mass approach. The backbones of all the structures generated give an identical fold with RMSDs on the average backbones within 0.5 Å. A total of 50 structures were generated by the simulated annealing protocol. 20 structures were then accepted for further analysis. The conformers generated were accepted on the basis of the lowest ROE violations. The analysis was carried out using the "accept.inp" routine included in the XPLOR software package. The 20 structures showed no violations of ROE constraints higher than 0.5 Å, bond angles higher than 5°, and bond lengths higher than 0.05 Å. The covalent geometry of the conformers generated was analyzed using PROCHECK_NMR.[39]

UV Spectroscopy and pK_A Determination. pH titrations were conducted to measure the pK_A of the tyrosine in peptide A and in tyrosine solutions. Changes in tyrosine protonation were monitored by measuring the absorbance at 270 (tyr) nm and dividing by the sum of the absorbance at 270 (tyr) and 295 (tyr⁻) nm.[14] A Hitachi U-3000 UV−visible spectrophotometer and 1 cm path length cuvettes were employed. The tyrosine or peptide concentration was 50 μM, and 10 mM MES−NaOH (pH 4.0−5.5), 10 mM HEPES−NaOH (pH 6.0−8.0), 10 mM boric acid−NaOH (8.5−10.5), or 10 mM CAPS−NaOH (pH 11.0−11.5) were employed as buffers. Experiments were performed on two different samples and then averaged. Experiments performed with a different choice of buffering agent gave the same result.

EPR Spectroscopy. The tyrosine or peptide A concentration was 1.0 mM, and either 10 mM sodium phosphate−NaOH (pH 5) or 10 mM boric acid−NaOH (pH 11) was used as a buffer. EPR spectra were collected on a Bruker EMX spectrometer (Billerica, MA). Spectra were recorded at 103 K through the use of a Wilmad (Buena, NJ) flow-through dewar. The radical was generated with a 266 nm photolysis pulse using methods previously described.[9] After baseline correction, spectra were integrated twice using Igor Pro software (Wavemetrics, Lake Oswego, OR). Experiments were performed on two different samples and averaged.

Electrochemistry. Tyrosine (0.01 mM), peptide A (0.05−0.1 mM), and peptide C (0.1 mM) samples were prepared in buffered solutions that contained 0.2 M KCl and 10 mM sodium acetate−NaOH (pH 4.0−5.5), 10 mM sodium phosphate (pH 6.0−7.8), 10 mM boric acid−NaOH (8.0−9.5), or 10 mM CAPS−NaOH (pH 10.0−11.8). Square

wave voltammetry measurements were performed on a computer-controlled CH Instruments, Inc. (Austin, TX) electrochemical workstation. The experiments were conducted in a three-electrode cell, equipped with a 3 mm diameter glassy carbon working electrode from Bioanalytical Systems, Inc. (West Lafayette, IN), a platinum foil counter electrode, and a reference electrode, Ag/AgCl in 1 M KCl, E = 0.22 V (NHE). In order to eliminate junction potential between the reference electrode and the test solution an electrolytic junction filled with 1 M KNO$_3$ was used. The sample was purged with nitrogen gas during data collection. Oxidation was initiated with a holding time of 2 s at 0.1 V and then scanned up to 1.1 V. Data were collected in increments of ΔE = 0.004 V. The square wave frequency, f, was 5 Hz, and the amplitude, A, of the applied pulse was 0.025 V (scan rate $\nu = f * A$ = 125 mV/s). The parameters were optimized in relation to the maximum value of peak current and peak width (half peak potential). The data were fit to a baseline manually, and the centroid was used to derive the peak potential. Experiments were performed on two to four samples and averaged, and experiments conducted with different buffers gave similar results. A standard, hexaamine ruthenium(III) chloride (Strem Chemicals, Newburyport, MA) at 2.5 mM in 1 N KCl, was run on each day of data acquisition. The averaged value for this standard was −0.18 ± 0.01 V. Experiments performed with a different choice of buffering agent gave the same result.

The pH dependence of the peak potential was analyzed using Igor Pro software. The data for tyrosine and peptide C were fit with the following equation: $E_m = E^* - 0.06 \log[\{10^{-pK^{ox}} + 10^{-pH}\}/\{10^{-pK^{red}} + 10^{-pH}\}]$, which describes the influence of a single protonatable group on the midpoint potential of a single electron-transfer reaction.[40,41] In this equation, E^* is the extrapolated midpoint potential at pH = 0, and pK^{ox} and pK^{red} are the pK_A values of the tyrosine side chain in the oxidized (tyrosyl radical) and reduced forms, respectively. In trial fits, E^* and pK^{red} were estimated from the data and then varied so as to minimize the chi-square value. In the resulting best fit to both the tyrosine and the peptide C data, pK^{ox} was equal to 0 (see ref 10) and pK^{red} was equal to 10.0 (see optical titration data, Figure 3). E^* was equal to 1.33 V for tyrosine and 1.28 V for peptide C. For peptide C, equations including the protonation of more than one titratable group gave a less reliable fit to the data, as assessed by the chi-square value.

For peptide A, data, describing the pH dependence of the peak potential, were fit with the following equation, $E_m = E^* - 0.06 \log [[(\{10^{-pH}\}^3 + \{10^{-pH}\}^2 * \{10^{-pK^{ox1}}\}) + (\{10^{-pH}\} * \{10^{-pK^{ox1}}\} * \{10^{-pK^{ox2}}\}) + (\{10^{-pK^{ox1}}\} * (10^{-pK^{ox2}}) * \{10^{-pK^{ox3}}\})]/[(\{10^{-pH}\}^3 + \{10^{-pH}\}^2 * \{10^{-pK^{red1}}\}) + (\{10^{-pH}\} * \{10^{-pK^{red1}}\} * \{10^{-pK^{red2}}\}) + (\{10^{-pK^{red1}}\} * (10^{-pK^{red2}}) * \{10^{-pK^{red3}}\})]]$, which describes the influence of three titratable groups on the midpoint potential of a one-electron-transfer reaction.[40,41] Initial values of the pK_A values were estimated from observed inflection points in the data, and the initial value of E^* was estimated by extrapolation. E^* and the pK_A values were then varied to optimize the chi-square value. In the final fit, the three values of pK^{ox} were equal to 0 (pK^{ox1}, assigned to tyrosine), 8.0 (pK^{ox2}, assigned to histidine), and 4.5 (pK^{ox3}, assigned to aspartic acid). The three values of pK^{red} were equal to 10.0 (pK^{red1}, assigned to tyrosine), 7.0 (pK^{red2}, assigned to histidine), and 4.0 (pK^{red3}, assigned to aspartic acid). In the final fit, E^* was equal to 1.09 V. Inclusion of only one or two titratable groups in the equation gave a less reliable fit to the data, as assessed by the chi-squared value.

Calculations. Electronic structure calculations were performed on gas-phase models of tyrosine and a tyrosyl radical with the Kohn−Sham density-functional theory (DFT) using the hybrid exchange functional of Becke[42,43] and the Lee, Yang, and Parr correlation functional[44] (B3LYP). All electronic structure calculations were

(35) Roberts, G. C. K. *NMR of macromolecules a practical approach*; Oxford University Press: New York, 1993.
(36) Brunger, A. T.; Adams, P. D.; Clore, G. M.; DeLano, W. L.; Gros, P.; Grosse-Kunstleve, R. W.; Jiang, J. S.; Kuszewski, J.; Nilges, M.; Pannu, N. S.; Read, R. J.; Rice, L. M.; Simonson, T.; Warren, G. L. *Acta Crystallogr., Sect. D* **1998**, *54*, 905−921.
(37) Schwieters, C. D.; Kuszewski, J. J.; Tjandra, N.; Clore, G. M. *J. Magn. Reson.* **2003**, *160*, 65−73.
(38) Nilges, M.; Gronenborn, A. M.; Brunger, A. T.; Clore, G. M. *Protein Eng.* **1988**, *2*, 27−38.
(39) Laskowski, R. A.; MacArthur, M. W.; Thornton, J. M. *Curr. Opin. Struct. Biol.* **1998**, *8*, 631−639.

(40) Clark, W. M. *Oxidation reduction potentials of organic systems*; The Williams and Wilkins Company: Baltimore, MD, 1960.
(41) Moore, G. R.; Pettigrew, G. W. *Cytochromes c. Evolutionary, Structural, and Physiochemical Aspects*; Springer-Verlag: Berlin, 1990.
(42) Becke, A. D. *J. Chem. Phys.* **1993**, *98*, 5648−5652.
(43) Becke, A. D. *Phys. Rev. A* **1988**, *38*, 3098−3100.
(44) Lee, C.; Yang, W.; Parr, R. G. *Phys. Rev. B* **1988**, *37*, 785−789.
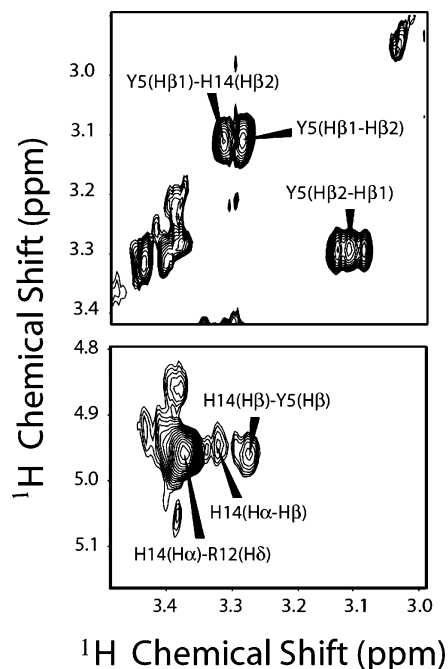
Figure 2. Portions of the $^1H/^1H$ ROESY spectrum acquired at 600 MHz showing the interstrand contacts between Y5 and H14 in peptide A. Dipolar correlations between β-protons (top panel) and between α- and β-protons (bottom panel) of Y5 and H14.

performed with the GAUSSIAN03 suite of programs.[45] The singlet tyrosine was modeled by an anionic tyrosine (with a proton on the phenolic oxygen) in the A conformation, as previously defined.[46] The tyrosyl radical was modeled by an anionic tyrosyl (with a deprotonated phenolic oxygen) in the A conformation.[46] The molecules are anionic due to the negative charge on the carboxylate group. These gas-phase model structures have been quite successful in previous studies of tyrosine and tyrosyl vibrational spectra.[46] Geometries were obtained using the 6-31++G(d,p) basis set,[47] as in ref 46. Integrals involving the exchange-correlation potential used the default numerical integration mesh with a maximum of 75 radial shells and 302 angular quadrature points per shell pruned to approximately 7000 points per atom.[48] Geometry optimizations were done in redundant internal coordinates with the default convergence criteria.[49] Maps of the electrostatic potential were created from B3LYP/6-311++G(3df,2p) single-point calculations.[47] The electrostatic potential was mapped onto an isodensity contour at 0.001 au using the gOpenMol suite of programs.[50]

Results and Discussion

Peptide A, IMDRYRVRNGDRIHIRLR (Figure 1A), was designed with an amino acid composition that promotes β-sheet formation,[51] an Asn-Gly type I′ turn sequence,[52] two salt bridges,[53] and a tyr−his aromatic interaction.[54] As a control, another peptide (peptide C) was synthesized in which His 14 was replaced with cyclohexylalanine (Cha).

(45) Frisch, et al. *Gaussian03*; Gaussian, Inc.: Wallingord, CT, 2004.
(46) Range, K.; Ayala, I.; York, D.; Barry, B. A. *J. Phys. Chem.* **2006**, *110*, 10970−10981.
(47) Frisch, M. J.; Pople, J. A.; Binkley, J. S. *J. Chem. Phys.* **1984**, *80*, 3265−3269.
(48) Frisch, A.; Frisch, M.; Trucks, G. W. *Gaussian03 User's Reference*; Gaussian, Inc.: Wallinford, CT, 2003.
(49) Peng, C.; Ayala, P. Y.; Schlegel, H. B.; Frisch, M. J. *J. Comput. Chem.* **1996**, *17*, 49−56.
(50) Laaksonen, L. *gOpenMol 3.00* (htpp://222/cac.fi/gopenmol/); 2005.
(51) Smith, C. K. W. J. M.; Regan, L. *Biochemistry* **1994**, *33*, 5510−5517.
(52) Griffiths-Jones, S. R. M. A. J.; Searle, M. S. *J. Mol. Biol.* **1999**, *292*, 1051−1069.
(53) Ciani, B. J. M.; Searle, M. *J. Am. Chem. Soc.* **2003**, *125*, 9038−9047.
(54) Kiehna, S. E.; Waters, M. L. *Protein Sci.* **2003**, *12*, 2657−2667.
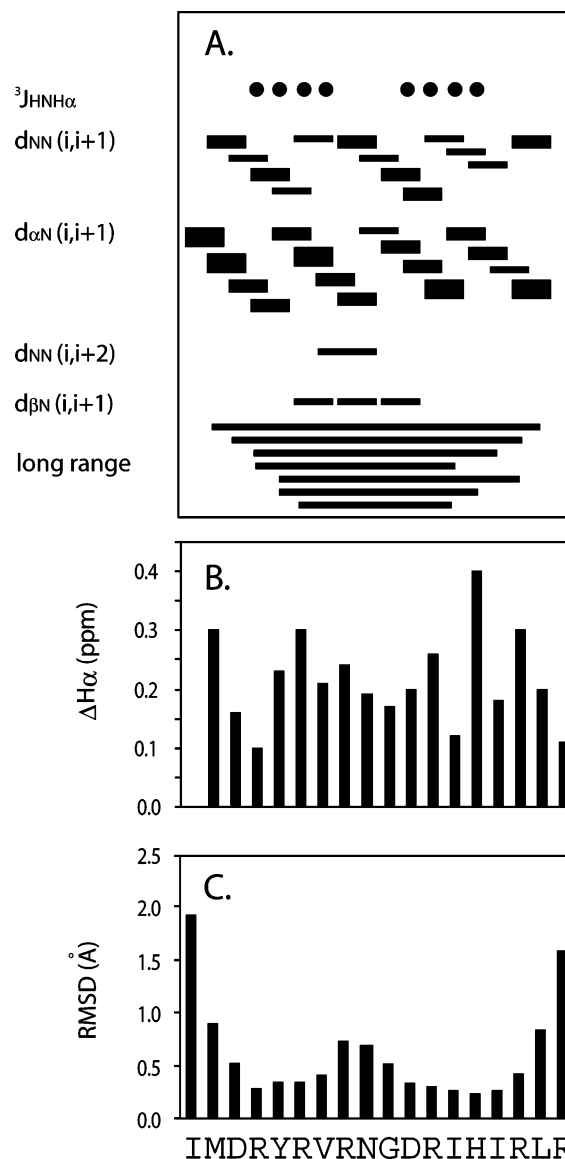
Figure 3. Summary of the NMR data: (A) short- and long-range ROEs, (B) the H_α chemical shift index, and (C) the root-mean-square deviations of the backbone atoms (C_α, NH, C′) for the conformational ensemble calculated using simulated annealing procedures. See Materials and Methods for more information and the Supporting information for a table of ROE values used in the simulated annealing.

NMR spectroscopy was used to determine the structure of peptide A at pH 5.0. Representative data and a complete list of all observed ROE values are presented in Figures 2 and 3 and in the Supporting Information. As predicted, the peptide forms a well-ordered β-hairpin (Figure 1B). The chemical shift index of H_α reported in Figure 3B displays only positive deviations from the random coil values. Excluding the terminal residues, an average of 10 ROEs per residues were detected, resulting in a well-ordered backbone structure with an ~0.5 Å RMSD (Figure 3C). A plot summarizing the backbone ROEs and $^3J_{HN-H\alpha}$ is reported in Figure 3A, while a complete table with all of the short- and long-range ROEs found for both the backbone and the side chains with the distance assigned is reported in the Supporting Information. The average minimized structure (Figure 1C) obtained from the simulated annealing calculations shows that the two aromatic residues Tyr 5 and His 14 are cofacially aligned. The interstrand ROEs between
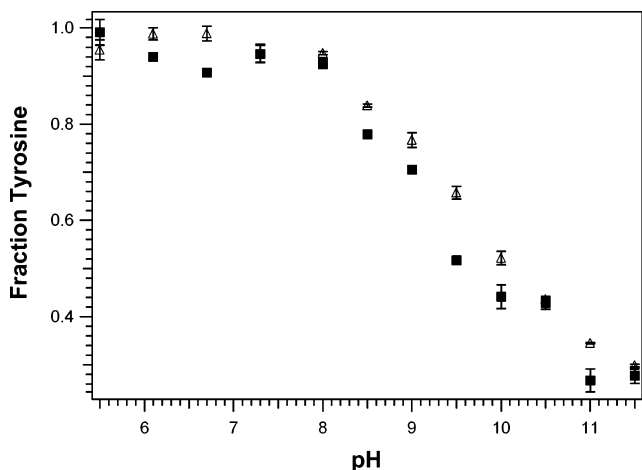
Figure 4. Optical titration of the peptide A (△) and tyrosine solutions (■). Fraction tyrosine is defined as [tyr]/{[tyr] + [tyr⁻]}.

Table 1. Electrochemical and EPR Studies of Peptide A and Tyrosine Samples

		voltammetry	EPR
sample	pH	peak potential[a] (V)	radical yield[b]
peptide A	5.0	0.97 ± 0.01	97 ± 12
tyrosine	5.0	1.02 ± 0.01	65 ± 9
peptide A	11.0	0.69 ± 0.01	119 ± 15
tyrosinate	11.0	0.70 ± 0.01	112 ± 10

[a] Peak potential versus NHE. [b] Relative yield derived by double integration of the tyrosyl radical EPR spectrum under nonsaturating conditions.

these residues are highlighted in Figure 2, showing that the distances between the protons of His 14 and Tyr 5 are less than 5 Å. This offset, stacked orientation is typical of $\pi-\pi$ interactions in proteins.[55] Tyr 5 is also located within ∼5 Å of Arg 16 and Asp 3. The average, minimized structure suggests that Arg 16 forms a salt bridge with the cross-strand Asp 3 (Figure 1C) and that Arg 16 forms a hydrogen bond to the Tyr 5 phenolic oxygen through the arginine ϵ-NH group (Figure 1C).

The effect of these intermolecular interactions on the pK_A of the tyrosine side chain in peptide A was investigated. This experiment was performed by monitoring the deprotonation of the tyrosine side chain through optical spectroscopy. There was no significant shift of the pK_A when tyrosine solutions were compared to peptide A (Figure 4). This can be rationalized by reference to the averaged and minimized peptide NMR structure (Figure 1C), which shows that the arginine, which is hydrogen bonded to the tyrosine, is also involved in a salt bridge with aspartate. The effect of this arginine−aspartate interaction is to neutralize the charge on the arginine side chain.

Tyrosine can be oxidized photochemically by 266 nm UV photolysis, and the resulting neutral radical can be detected and quantitated by EPR spectroscopy (Figure 5). Microwave power saturation curves for tyrosine and peptide A samples were measured at both pH 5 and pH 11. These experiments showed that the $P_{1/2}$ values for the tyrosyl radical in the tyrosine and peptide samples were significantly altered, when the two samples are compared. For peptide A, the values were 1.8 mW at pH 11 and 1.6 mW at pH 5.0. For tyrosine, the values were 0.5 mW at pH 11 and 0.7 mW at pH 5. Accordingly, EPR
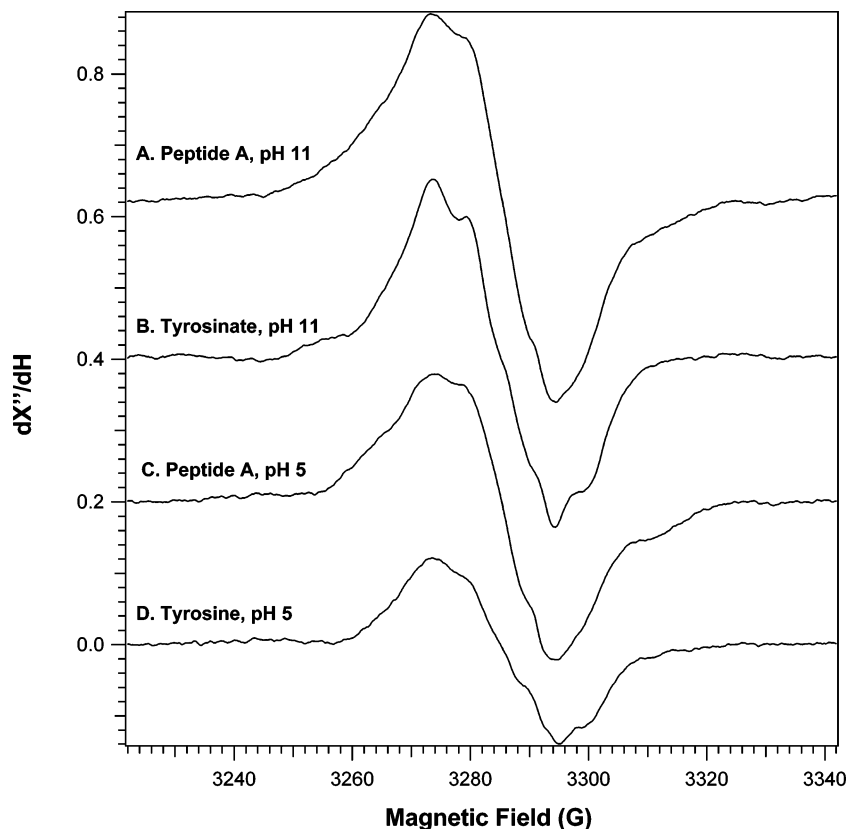

Figure 5. EPR spectra of tyrosyl radical, generated by UV photolysis, in peptide A at pH 11 (A) and pH 5 (C). For comparison, spectra generated from tyrosinate at pH 11 (B) and from tyrosine at pH 5 (D) are also shown. Spectral conditions were as follows: microwave frequency, 9.21 GHz; power, 200 μW; modulation amplitude, 3 G; modulation frequency, 100 kHz; time constant, 655.36 ms; conversion time, 163.84 ms; number of scans, 4; temperature, 103 K.
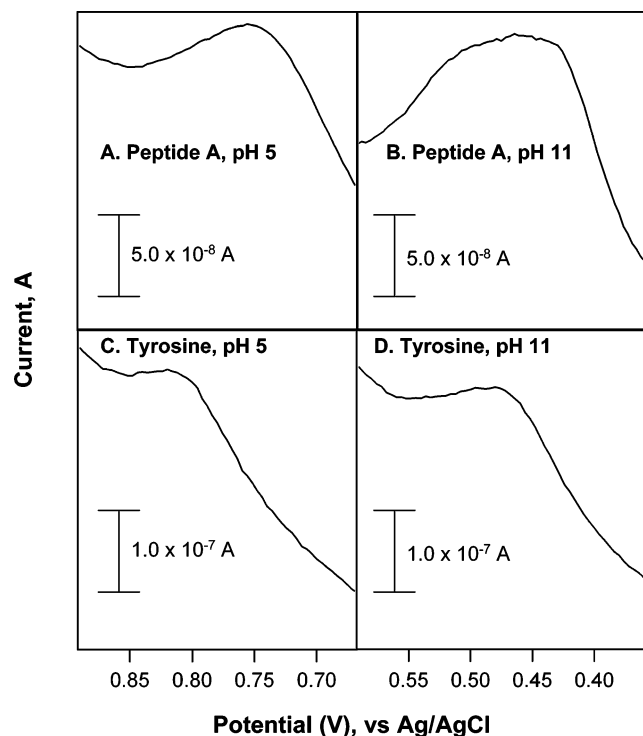
Figure 6. Square wave voltammetry on tyrosine and peptide A solutions. The anodic current versus applied potential are plotted for tyrosine at pH 5 (C) and pH 11 (D) and for peptide A at pH 5 (A) and pH 11 (B). For the assignment of peak potentials, see Table 1. Experimental conditions are reported in the Materials and Methods section.

experiments were conducted at 0.2 mW, at which no significant saturation or power broadening would be expected in either sample. The difference in $P_{1/2}$, when the tyrosine and peptide A samples are compared, provides support for the conclusion that the peptide tyrosyl radical is involved in an interstrand, noncovalent interaction at both pH values and is not in an exclusively aqueous environment.

Under nonsaturating microwave power conditions at 0.2 mW, the EPR spectra recorded in tyrosine (Figure 5B and D) and peptide A (Figure 5A and C) samples showed small differences in line shape, which mainly corresponded to broadening of the peptide A EPR line shape. Observed differences in the EPR signals (Figure 5) are consistent with a difference in the distribution of side chain conformers in the peptide or with a redistribution of spin density, which could be caused by hydrogen bonding between the arginine side chain and the tyrosyl radical.[7,9] The origin of this effect is interesting and can be pursued by eventual isotopic labeling of the tyrosyl radical in peptide A and by EPR simulations. A contribution to the EPR spectrum from an oxidized histidine side chain is unlikely due to the reported redox potentials of histidine and tyrosine.[56,57]

The EPR spectra were doubly integrated in order to quantitate the amount of signal. The 266 nm optical properties of the samples at 103 K were similar. The results show that, at pH 11, the yield of the neutral radical was indistinguishable in peptide A and tyrosine (Figure 5A and B, Table 1). However, there was a significant increase in radical yield in the peptide at pH 5.0, relative to tyrosine were solutions (Figure 5C and D, Table 1). There was no significant change in the extinction
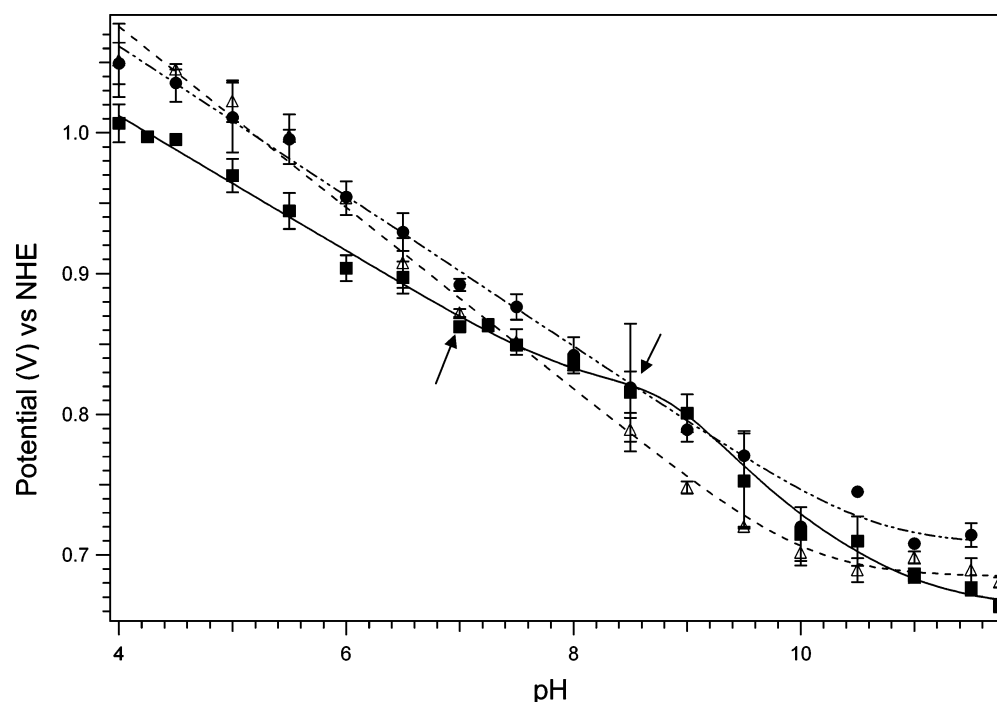

Figure 7. Effect of pH on the peak potential of the anodic waves, as assessed by square wave voltammetry, for peptide A (■), peptide C (●), and tyrosine solutions (△). In some cases, the error bars are smaller than the symbols used to represent the points. Data were fit with equations describing a model in which oxidation is coupled to protonation of one (peptide C, dot-dashed line and tyrosine, dashed line) or three (peptide A, solid line) ionizable groups.[40,41] See the Materials and Methods section for details concerning the fits. As expected, the tyrosine and peptide C data (△ and ●, respectively) were fit well with a model in which protonation of the tyrosine phenolic oxygen ($pK_A = 0$, oxidized state and 10, reduced state) influences the potential (dashed and dot-dashed lines). Peptide A data were fit best with a model in which three ionizable groups influence the potential (solid line). In peptide A (solid line), pK_A values of 0 (oxidized state) and 10 (reduced state) were attributed to tyr, pK_A values of 8.0 (oxidized state) and 7.0 (reduced state) were attributed to his, and pK_A values of 4.5 (oxidized state) and 4.0 (reduced state) were attributed to an aspartic acid. The arrows show inflection points assigned to histidine in peptide A.
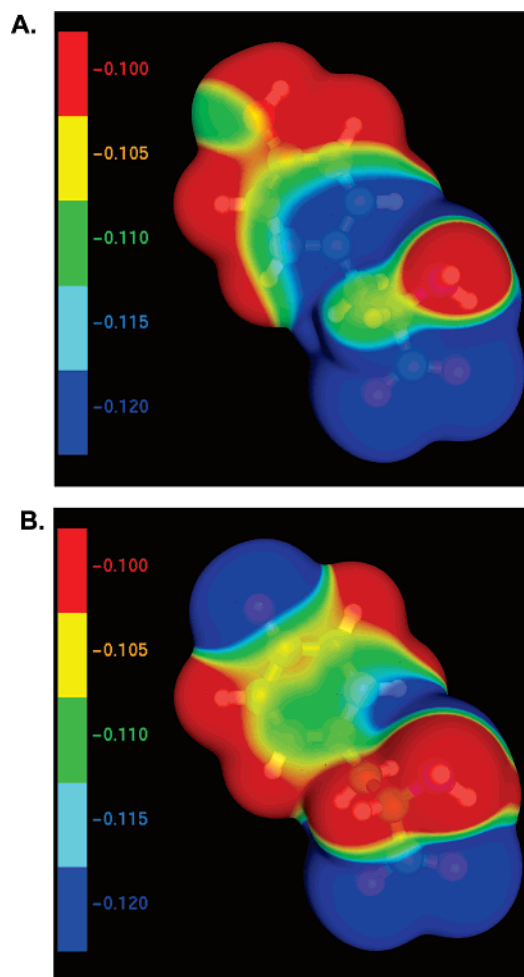
Figure 8. Electrostatic maps of tyrosine (A) and the tyrosyl radical (B) in their anionic forms. The molecules are anionic due to the negative charge on the carboxylate group. The colors correspond to the value of the electrostatic potential in atomic units; red colors are more positive, and blue colors are more negative.

coefficient at 266 nm, when peptide A and tyrosine were compared (data not shown). This is expected because histidine has no significant absorption at this wavelength, at either pH 5 or pH 11 (data not shown). These EPR results could be consistent with a change in the redox potential of the tyrosine side chain at low pH, if there is no difference in nonradiative decay rate. Upon photoionization of tyrosine at room temperature, the solvated electron can be detected optically, so the eventual electron acceptor in both samples is likely to be solvent {reviewed in ref 1}. The issue of the nonradiative decay rate can be pursued in future experiments. At pH 11, the NMR spectrum shows no collapse of the Hα region, indicating that the peptide is folded (Figure S2, Supporting Information). FT–IR measurements at a concentration of 50 mM also provide evidence for β-strand content at pH 11 (Figure S1, Supporting Information).

To test the idea that there is a change in tyrosine redox potential in peptide A, square wave voltammetry was employed {see refs 14,57}. Representative voltammograms for tyrosine and peptide A are presented in Figure 6. The tyrosine oxidation reaction has been shown to be irreversible in voltammetric experiments, but in previous work, the observed peak potentials can be corrected to give redox potentials.[57] In our experiments, there was no significant (<2%) effect of scan rate and

concentration on the measured potentials for peptide A,[14] suggesting that any correction factor is negligible. In previous work on a tyrosine-containing designed peptide, the correction was reported as 0.02 V.[14] Because we are not deriving any thermodynamic quantities in our analysis of the electrochemical data, we report the uncorrected peak potentials. For tyrosine, data had to be recorded at a low concentration to avoid increased data scatter due to a putative sample–electrode interaction. The potential for tyrosine at pH 7 was in good agreement with results in ref 57 after correction for NHE (+0.22V), when the same concentration was used.[58]

In Figure 7, the peak potential of tyrosine was determined as a function of pH at pH values between 4 and 12. For tyrosine solutions, the results (Figure 7, open triangles) show that, as expected, the potential increases linearly with decreasing pH under the pK_A (10.0) of the tyrosine phenolic oxygen. The observed, absolute value of the slope between pH 4 and 10 is 63 mV/pH unit. This slope is in reasonable agreement with the expected slope (59 mV/pH unit) for an electron-transfer process in which both a proton and an electron are transferred at 25 °C.[57] The data were fit (Figure 7, open triangles, dashed line) with a modified Nernst equation, in which it is assumed that a single proton-transfer reaction, in this case, the protonation of the tyrosine side chain, influences the potential.[40,41] However, the pH dependence of the peak potential (Figure 7, squares) for tyrosine-containing peptide A reveals a more complex reaction process. Peptide A data were fit best with a model in which three ionizable groups, attributed to aspartic acid, histidine, and tyrosine, influence the potential (solid line). In particular, two pK_A values of 7.0 and 8.0 are evident as inflection points (Figure 7, arrows) in the data.[41] These pK_A values are attributed to the cross-strand histidine (His 14), which has dipolar contacts with the tyrosine side chain (Tyr5) (Figure 1B and C). This conclusion is supported by studies of peptide C, a peptide A variant in which cyclohexylalanine is substituted for His 14 and in which these turning points are not observed (Figure 7, circles, dot-dashed line). From the slope change at each inflection point, the value of 7.0 is assigned to the pK_A of His14 in the reduced state and the value of 8.0 is assigned to the pK_A of His14 in the oxidized state {see ref 41 and references therein}. In peptide A (solid line), pK_A values of 0 (oxidized state) and 10 (reduced state) were attributed to Tyr5, and pK_A values of 4.5 (oxidized state) and 4.0 (reduced state) were attributed to Asp3.

A pK_A of 7.0 is typical of the histidine side chain in proteins. As observed in Figure 7 and the associated fit, when the tyrosine side chain in peptide A is oxidized, the pK_A of the histidine increases by ~1 pH unit. Therefore, in the pH range from 7.0 to 8.0, the histidine side chain protonates when the tyrosine side chain is oxidized, and the oxidation reaction between pH 7.0 and 8.0 results in the net transfer of a proton from the tyrosine to the histidine. In the ranges from pH 8.0–10.0 and 4.5–6.9 (Figure 7), the absolute values of linear slopes derived from the data are 51 ± 9 mV/pH unit and 53 ± 3 mV/pH unit, respectively. As stated above, these values are consistent with the expected one proton–one electron reaction. The change in

(55) Waters, M. L. *Curr. Opin. Chem. Biol.* **2002**, *6*, 736−741.
(56) Brabec, V.; Mornstein, V. *Biophys. Chem.* **1980**, *12*, 159−165.
(57) Harriman, A. *J. Phys. Chem.* **1987**, *91*, 6102−6104.
(58) Dean, J. A. *Lange's Handbook of Chemistry*; Mcgraw-Hill Inc.: New York, 1999.

slope (to 27 ± 6 mV/pH unit) in the pH range between 7.0 and 8.0 may be due to the close overlap of the histidine pK_A values.

As observed in Table 1, the consequence of this proton-coupled electron-transfer reaction is to favor tyrosyl radical formation at low pH. If one considers thermodynamic linkage of the oxidation and reduction reactions, the expected alteration in midpoint potential for a one unit pK_A change is a decrease of 59 mV at 25 °C $\{nF\Delta E_m = RT \ln(K_{ox}/K_{red})\}$.[11,41] When tyrosine and peptide A are compared, a 0.050 V decrease in peak potential in peptide A is observed at pH 5 (Table 1). This difference is significant compared to the 95% confidence intervals of each data set (data not shown). Moreover, the cyclohexylalanine variant shows a confirmatory increase in peak potential at low pH, when compared to peptide A (Figure 7, circles). Taken together, these data suggest that histidine protonation and tyrosine oxidation are thermodynamically linked in peptide A.

Our results show that peptide bond formation and proton transfer involving histidine can alter the redox potential of tyrosine, even when the histidine and tyrosine are not directly hydrogen bonded. To understand the basis of this interaction, electrostatic maps were calculated[46] for tyrosine (Figure 8A) and for the tyrosyl radical (Figure 8B). As observed in Figure 8, oxidation of tyrosine is associated with an increase in negative charge on the phenolic oxygen, which may stabilize the positive charge on the histidine side chain. In turn, the protonated imidazole group will stabilize the tyrosyl radical, relative to tyrosine, through a π−cation interaction. Thus, our results suggest a novel method by which the protein environment can alter tyrosyl radical function and control electron-transfer rates.

Supporting Information Available: Complete ref 45, the ROEs used in the simulated annealing procedure, the Hα region of the peptide A NMR spectrum at pH 11, and a peptide A FT−IR spectrum at pH 11. This material is available free of charge via the Internet at http://pubs.acs.org.

JA068805F